Magnetic ordering and exchange interactions in structural modifications of Mn_3Ga alloys: Interplay of frustration, atomic order, and off-stoichiometry

Sergii Khmelevskyi,[1] Andrei V. Ruban,[2] and Peter Mohn[1]

[1]*Center for Computational Materials Science, Institute for Applied Physics, Vienna University of Technology, Wiedner Hauptstrasse 8, A-1040 Vienna, Austria*

[2]*Department of Materials Science and Engineering, Royal Institute of Technology, 10044 Stockholm, Sweden*

(Received 24 February 2016; revised manuscript received 13 April 2016; published 4 May 2016)

Mn-Ga alloys close to the Mn_3Ga stoichiometry can be synthesized in three different crystal modifications: hexagonal, tetragonal, and face-centered cubic, both in bulk and in thin-film forms. The magnetic ordering of these modifications is varying from noncollinear antiferromagnetic in the hexagonal case to ferrimagnetic order in the tetragonal one, whereas it is still unknown for the atomically disordered fcc structure. Here we study the onset of magnetic order at finite temperatures in these systems on a first-principles basis calculating the interatomic magnetic exchange interactions in the high-temperature paramagnetic regime. We employ the disordered local moment formalism and the magnetic force theorem within the framework of the local spin-density approximation and Monte Carlo simulations taking also the effects of atomic disorder in fcc alloys into account. In particular we find the origin of the stabilization of the noncollinear 3*k* structure in competition between antiferromagnetic inter- and in-plane couplings of frustrated kagome planes in hexagonal Mn_3Ga and predict the antiferromagnetic-1 collinear order due to frustration in fcc alloys. Special attention is paid to the effects of the off-stoichiometry and the consequences of atomic disorder. We calculate the site-preference energy of Ga antisite atoms in the tetragonal structures in the range of the compositions from Mn_3Ga to Mn_2Ga and slightly beyond and confirm the earlier explanation of the effect of magnetization increase due to Ga preferentially occupying one of the Mn sites.

DOI: 10.1103/PhysRevB.93.184404

I. INTRODUCTION

Recent developments in spintronics, such as spin valves (SVs) and magnetic tunnel junctions (MTJs) [1] led to an increasing demand for magnetic materials, which satisfy stringent technological requirements: high ordering temperatures, magnetic anisotropy, structural thermal stability, etc. In particular, there is a growing interest in the novel high-temperature antiferromagnetic (AFM) materials with high magnetic anisotropy, which can replace the currently used alloys containing expensive constituents, such as Ir, used as pinning layers in functional SVs and MTJs. On the other hand, the ferromagnetic materials for thin films with high and thermally stable perpendicular magnetic anisotropy as well as high-temperature ferrimagnets for fast magnetization switching and giant magnetoresistance ratio are continuously in the focus of the spintronic research.

It is thus not surprising that the magnetism of Mn_3Ga alloys and thin films have been intensively studied during recent years both experimentally and theoretically (see for an overview Refs. [2,3]) as their different crystal modifications can be utilized for different purposes. The bulk [4,5] and thin films of this material can be experimentally stabilized [6,7] in the hexagonal DO_{19} crystal structure ε-Mn_3Ga, which is antiferromagnetic with a high Néel temperature at about 470 K [4], and a noncollinear triangular magnetic structure [4,7] similar to the triangular magnetic state in the archetypical $IrMn_3$ functional antiferromagnet [8]. It has been demonstrated recently that exchange-biased MTJs with antiferromagnetic ε-Mn_3Ga have remarkably large values of the exchange bias field due to a frustrated triangular AFM structure, comparably to other MTJs without heavy elements, such as Ir and Pt [7]. On the other hand, the tetragonal phase of Mn_3Ga with the DO_{22} structure (τ phase) is a relatively novel hard magnetic material [9], which has a high uniaxial anisotropy and Curie temperature of about 770 K depending on the stoichiometry [6,9]. The τ-Mn_3Ga phase can be derived by annealing the hexagonal material in bulk and thin-film forms. The magnetic properties of the Mn-Ga tetragonal phase are found to be very promising for various applications in SVs and MTJs [2,6]. This has triggered an intensive experimental investigation of the bulk [9] and thin films grown on various substrates [6,10–13]. Such magnetic properties of the tetragonal Mn_3Ga films as magnetization and anisotropy however strongly depend on the stoichiometry of the $Mn_{3-x}Ga$ alloys and the preparation conditions [10,13]. It is interesting that the magnetization increases almost linearly with manganese deficiency up to the composition of Mn_2Ga where the alloys retain the tetragonal structure [10]. This effect is related to the preferential site occupation of the excess of the Ga antisite (AS) atoms on the two nonequivalent Mn positions in the DO_{22} structure and the ferrimagnetic character of the order between these two sites [6,13,14] (see also Sec. IV). However, the latest neutron-diffraction experiments indicate the presence of a magnetic noncollinear structure (with small canting of the moments on one of the Mn sublattices) in the atomically well-ordered $Mn_{3-x}Ga$ close to the ideal Mn_3Ga stoichiometry [13]. This property has been claimed to be intrinsic and not related to the formation of a secondary phase [13]. In fact, it

appears that the interplay of the atomic composition, atomic disorder, and magnetic interactions in the τ-$Mn_{3-x}Ga$ phase are by no means trivial at all.

There exist quite elaborate first-principles studies of the tetragonal Mn_3Ga alloy [9,13–17], however the investigations of the hexagonal phase are scarce [18]. Electronic structure calculations within the local spin-density approximation (LSDA) predict a ferrimagnetic ground state in the stoichiometric τ-Mn_3Ga with antiparallel orientation of the moments in the Mn $2b$ and $4d$ sites of the tetragonal DO_{22} structure [9,16]. The electronic structure of alloys based on the tetragonal Mn_3Ga has been extensively investigated by Chadov *et al.* [17] in an attempt to determine the effect of alloying on its physical properties. The τ-$Mn_{3-x}Ga$ with an excess of the Ga together with the strain effects on the magnetic structure of $Mn_{3-x}Ga$ films have been studied in first-principles calculations in Ref. [14] where it has been demonstrated that the total magnetization in tetragonal $Mn_{3-x}Ga$ increases with decreasing Mn due to preferential occupation of Mn-$2b$ sites by Ga earlier suggested in Ref. [9]. In this paper, we will explore this topic further determining the site preference of Ga in the ordered and thermally disordered magnetic state. Magnetic exchange interactions in fully stoichiometric τ-Mn_3Ga have been obtained independently by Kübler [15] and Rode *et al.* [13] using a mapping of the spin-spiral energies onto a Heisenberg model. The ferrimagnetic ordering temperatures within the random-phase approximation (RPA) obtained in these papers are 762 K [15] and 670 K [13], which are close to the experimental estimate of about 770 K [9]. Strong antiferromagnetic coupling between the Mn moments on the $4d$ and $2b$ sites of the DO_{22} structure constrains the collinear ferromagnetic state, and thus the origin of the recently reported canted magnetic structure [13] remains unclear (see the discussion in Sec. III).

First-principles calculations [18] predict the complex magnetic structure of the hexagonal ε-Mn_3Ga phase in agreement with experiment. The exchange interactions and the Néel temperature, however, have not been estimated from first-principles calculations until the present. It was suggested [19,20] that the origin of the special kind of magnetic order found in ε-Mn_3Ga is the result of the geometrical frustration on the kagome basal planes together with the strong Dzyaloshinskii-Moriya (DM) interaction [5]. The effect of frustrations on the kagome lattice is a highly interesting topic on its own. As is demonstrated in Sec. IV, the triangular order where the nearest-neighbor (NN) Mn moments have angles of 120° in-plane as well as out of the kagome planes is the result of the competition of the purely isotropic (nonrelativistic) exchange interactions.

There is another important topic connected with Mn-Ga alloys, which has been largely inspired by *ab initio* calculations, which predict a half-metallic electronic structure in Mn_3Ga having a full Heusler structure [21]. In general, there was a larger number of studies of various Heusler alloys and related tetragonal distorted structures based on Mn and Ga, which resulted in the invention of various promising functional materials [22]. Notable recent experimental progress in this direction led to the stabilization of half-Heusler Mn_2Ga thin films doped with Ru [23].

The cubic phase of Mn_3Ga has been experimentally produced and investigated only very recently [24]. It has a disordered face-centered-cubic (fcc) structure, which is magnetically ordered at room temperature with zero net magnetization. The exact type of magnetic order in disordered fcc Mn_3Ga is still unknown, although the calculations performed with a large fcc-based supercell structures have suggested [24] antiferromagnetic coupling between nearest-neighbor Mn moments. It is interesting to note that similar to the hexagonal Mn_3Ga the disordered fcc lattice is geometrically frustrated. Moreover, the fcc lattice can be viewed as a set of the triangular (111) planes, similar to the magnetic sublattice of the hexagonal DO_{19} structure, which is composed of alternating basal kagome planes along the c direction. Removing one magnetic site from the fcc lattice (e.g., due to Cu_3Au-type ordering) the resulting magnetic sublattice would be similar to the one in hexagonal Mn_3Ga. Here, we will show that the frustration between AFM interactions in the fcc Mn_3Ga structure leads to a quite different magnetic order from that in ε-Mn_3Ga.

The aim of the present paper is to investigate the formation of the magnetic order in all three known crystalline modifications of Mn_3Ga (and compositions close to stoichiometry) within the same theoretical first-principles scheme based on calculations of the interatomic exchange interactions in the paramagnetic (PM) state with disordered local moments and statistical simulations employing a Monte Carlo (MC) method on ordered and site-disordered lattices. The calculated exchange constants allow the prediction of the magnetic ordering temperature with reasonable accuracy for the tetragonal and hexagonal phases and reveal the mechanism of the stabilization of the triangular magnetic state in the system of frustrated kagome planes. The interesting finding is that due to the presence of nonmagnetic Ga there are two nonequivalent nearest-neighbor couplings on the kagome plane. We predict that in turn the disordered fcc phase would have an antiferromagnetic structure with alternating ordering of ferromagnetic [100] planes, so-called "kind-1" [25] or "AFM-1" [26] ordering on the fcc lattice. The ordering temperature of the fcc phase was predicted to be at about room temperature. The effects of the off-stoichiometry have been studied in detail for the tetragonal phase.

II. METHODOLOGY AND COMPUTATIONAL DETAILS

Our first-principles investigation is based on the LSDA [27] and the Korringa-Kohn-Rostoker (KKR) method in the atomic sphere approximation (ASA) [28,29]. For calculation of the electronic structure of alloys with atomic disorder a single-site coherent potential approximation (CPA) [29] was used. The partial waves in the KKR-ASA calculations have been expanded up to $l_{\max} = 3$ (*spdf* – basis) inside the atomic spheres. The radii of the ASA spheres were set equal for all nonequivalent atomic sites.

In this paper, we have used the experimental lattice parameters: $a = 3.777$ Å for the disordered fcc phase [24]; $a = 3.91$ and $c = 7.12$ Å for the tetragonal τ phase; and $a = 5.404$ and $c = 4.357$ Å for the hexagonal ε phase [6].

The magnetic exchange interactions J_{ij} of the classical Heisenberg Hamiltonian,

$$H = -\sum_{i,j\in\{\mathrm{Mn}\}} J_{ij}\vec{e}_i\vec{e}_j, \quad (1)$$

where $\vec{e}_i$ is the unit directional vector of the magnetic moment at the ith Mn lattice site have been calculated using the magnetic force theorem [30] embedded [31] in the bulk Korringa-Kohn-Rostoker band-structure method. The exchange interactions were estimated in the paramagnetic disordered local moment (DLM) state, which is a model for the magnetic disorder above the magnetic ordering temperature [32]. Indeed, the importance of using the DLM reference state for calculating magnetic transitions will be demonstrated in Sec. III, where we compare the results obtained in the DLM state with the exchange interactions for the low-temperature ground state.

The Monte Carlo simulations with Hamiltonian (1) have been performed for a sample consisting of about 10^4 magnetic sites using periodic boundary conditions and a conventional Metropolis algorithm. A Monte Carlo simulation for the fcc random $Mn_{75}Ga_{25}$ alloy has been performed using a supercell with Mn atoms distributed by a random number generator on the fcc lattice.

This methodology has been previously successfully used in the description of the magnetism in various Mn-based systems. In particular, we theoretically predicted the high-temperature antiferromagnetism and magnetic structure in a tetragonal Mn_2Au compound [33], which has been confirmed in a recent experiment [34]. We also investigated the effects of magnetic frustrations and atomic disorder on the Néel temperature in cubic $Ru_2Mn(Ga,Si,Ge)$ Heusler alloys [35] and in NiMnSb half-Heusler alloys [36] where the magnetic Mn occupies the frustrated fcc sublattice.

III. TETRAGONAL τ-$Mn_{3-x}Ga$ PHASE

A. Stoichiometric ordered alloy

The DO_{22} crystal structure of the tetragonal τ phase of Mn_3Ga is shown in Fig. 1. Mn atoms occupy the two nonequivalent positions $2b$ and $4d$. This structure can be viewed as a strongly tetragonally distorted $L2_1$ full Heusler structure (X_2YZ with $X = Y$). The cubic symmetry is recovered if $c = \sqrt{2}a$, however, tetragonal distortion with respect to a cubic Heusler structure in the case of Mn_3Ga is at about 1.28. Therefore it is not surprising that experimental attempts to synthesize the cubic $L2_1$ phase, which according to the theory [16] will be a half-metallic fully compensated antiferromagnet, failed and a different cubic structure (Cu_3Au-type) was stabilized instead [24].

In the high-temperature paramagnetic DLM state the Mn moments are calculated to be 2.43 μ_B/Mn on the $2b$ positions and 2.53 μ_B/Mn on the $4d$ positions, whereas in the ordered ground state the moments are -2.99 μ_B/Mn and 2.38 μ_B/Mn on both positions, respectively, and have the antiparallel orientation (ferrimagnetic state). The latter magnitudes are very close to those observed in neutron-diffraction experiments [13]. One notices that, in the magnetically disordered state, the difference between the magnetic moments of the two sites

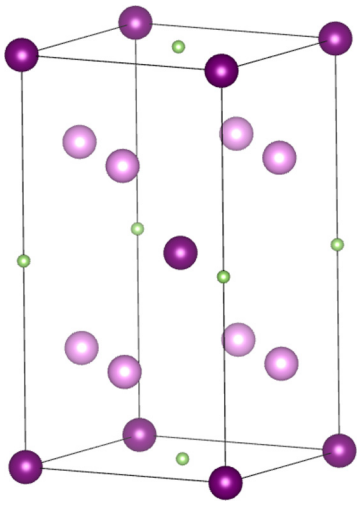

FIG. 1. The DO_{22} structure of Mn_3Ga. The big circles are Mn (the darker ones are the $2b$, and the lighter ones are the $4d$ sites), and the small circles are the nonmagnetic Ga atoms.

is much smaller than in the ordered case since the absolute value of the moment on Mn($2b$) is sensitive to the magnetic environment. This indicates the limited applicability of the Heisenberg model with constant and temperature-independent exchange interactions. The tetragonal Mn_3Ga is thus an example of a system where the magnitude of the local moment depends on the state of magnetic disorder, and to correctly estimate the magnetic ordering temperature and type of order at finite temperatures one needs to calculate the exchange interactions in the DLM state [35,37].

In Fig. 2, we show magnetic exchange interactions in the paramagnetic DLM and ferrimagnetic states obtained as described in the previous section. In the DLM state, the dominating interaction is antiferromagnetic between $2b$-$4d$

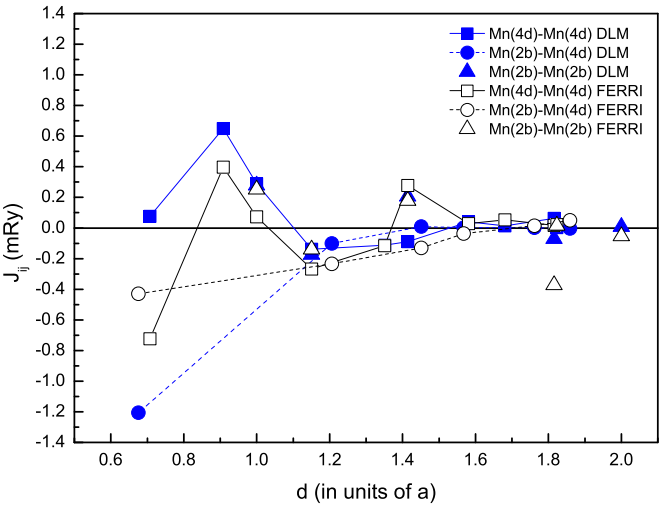

FIG. 2. Magnetic exchange interactions calculated in the DLM paramgnetic state (filled symbols) and in the fully ordered ferrimagnetic state (open symbols) plotted as a function of the interatomic distance. Squares, circles, and triangles are Mn($4d$)-Mn($4d$), Mn($2b$)-Mn($4d$), and Mn($2b$)-Mn($4d$) interactions, respectively.

nearest neighbors. At the same time, the nearest-neighbor 4*d*-4*d* interaction is ferromagnetic, but it is rather weak. Each of the Mn(2*b*) sites has eight Mn(4*d*) nearest neighbors, which together with quite strong ferromagnetic interactions at the second coordination shell for both 2*b* and 4*d* sublattices leads to the ferrimagnetic ordering at an elevated temperature. A similar behavior of the exchange interactions is seen from the fit to the calculated energies of the spin-spiral configurations in Ref. [13]. Our Monte Carlo simulations with the calculated DLM exchange constants (Fig. 2) yield the Néel temperature of 685 K, which is similar to the one obtained using the random-phase approximation (670 K) as given in Ref. [13]. Using the same exchange constants as given in Ref. [13] we also arrive at a similar value by performing a Monte Carlo simulation (675 K). At the same time, the exact experimental value of the ordering temperature can be estimated only approximately since the tetragonal phase undergoes a structural transformation into the hexagonal phase at a temperature just below the magnetic ordering temperature. A rough estimate however, suggests that it should be around 770 K [6]. The agreement between theory and experiment can be considered as rather fair, owing to the known slight underestimation of the magnetic ordering temperatures in Mn-based intermetallics with large local moments [35] due to omitting the moderate local correlation effects in LSDA and the use of the classical Heisenberg Hamiltonian (see, e.g., Refs. [38,39]). In both cases (DLM and spin-spiral methods) the transition is found to be between paramagnetic and ferrimagnetic states, which is stable down to the lowest temperatures. Thus the isotropic nonrelativistic exchange constants do not explain the small canting of the 2*b* moments found in neutron-diffraction experiments [13]. The distant small antiferromagnetic interactions, which, as suggested in Ref. [13], together with the in-plane magnetic anisotropy of the 2*b* sites might be responsible for canting, cannot overthrow the strong first NN AFM coupling. This conclusion is directly supported by the results of the total energy calculations of the canted noncollinear magnetic states presented in Ref. [13], which has a minimum for the collinear spin-moment configuration.

The calculated exchange interactions in the ferrimagnetic state (Fig. 2, open symbols) differ substantially from the DLM interactions. The MC simulations with these constants produce the much lower ordering temperature (540 K). Although they might be more relevant for magnetic excitations at low temperatures, they are less accurate than DLM interactions for temperatures close and above the Néel temperature.

B. Effects of off-stoichiometry

The bulk and thin-film samples of the τ-Mn_3Ga phase are usually Mn deficient [6,13,14], and they can be synthesized close to the stoichiometry of Mn_2Ga. It is found that the less Mn is in the sample the larger the measured saturated magnetization becomes [6,9,12,14]. This effect can be explained by the preferential occupation of Ga excess atoms of the Mn(2*b*) positions [9,14], which results in a decreasing magnetization of the Mn(2*b*) sublattice oriented oppositely to the magnetization of the Mn(4*d*) sublattice remaining unchanged upon doping.

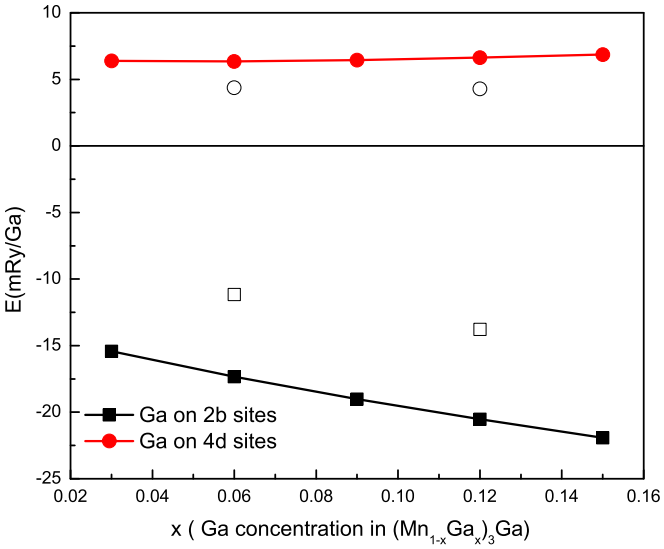

FIG. 3. Total energies of the off-stoichiometric $Mn_{3-x}Ga$ alloys calculated with different Ga distributions on Mn sites. The energies are given with respect to the alloy with fully random Ga distribution over the 2*b* and 4*d* sites and per one Ga antisite atom (site-preference energies). The squares denote excess Ga atoms on 2*b* sites. The circles denote excess Ga atoms on 4*d* sites. The open symbols are the energies calculated in the high-temperature paramagnetic state (DLM), and the filled circles are energies in the ferrimagnetic state.

Here, we calculate the site-preference energies for the Ga excess atoms in the DO_{22} structure, Mn atomic moments, and magnetization in the ferrimagnetic state in off-stoichiometric alloys in the framework of the CPA. In Fig. 3, we show the total energies of the $(Mn_{1-x}Ga_x)_3Ga$ alloys calculated for three different distributions of Ga atoms on the Mn sublattices: all excess (with respect to Mn_3Ga stoichiometry) AS-Ga atoms on 2*b* sites, all Ga-AS on 4*d* sites, and the Ga-AS are equally distributed over the Mn sites. The energies are given per single AS atom and with respect to the latter distribution case. One can see that Ga indeed prefers 2*b* sites (Fig. 3). Since the production of the τ phase is usually performed by annealing at elevated temperatures, we show the site-preference energies calculated both in the low-temperature ferromagnetic state (full symbols) and in the high-temperature DLM state (open symbols). For both cases we find that excess Ga atoms strongly prefer the Mn(2*b*) positions. At usual annealing temperatures of 400–500 K ($\sim$3 mRy) almost all Ga-AS would populate 2*b* sites. The calculated magnetic moments and magnetization in alloys with such Ga distributions are shown in Fig. 4. One can see that the moments on both Mn sites remain almost unchanged with increasing Ga concentration resulting in an almost linear total magnetization increase. The other scenario, namely, that Mn disappears from 2*b* positions leaving vacancies in off-stoichiometric samples can be completely ruled out since it is energetically highly unfavorable. For instance, the calculated energy cost of creating composition compensating (or structural) vacancies on Mn sites instead of creating Ga-AS on the Mn(2*b*) sublattice is $\sim$180 mRy per vacancy on the Mn 2*b* sites.

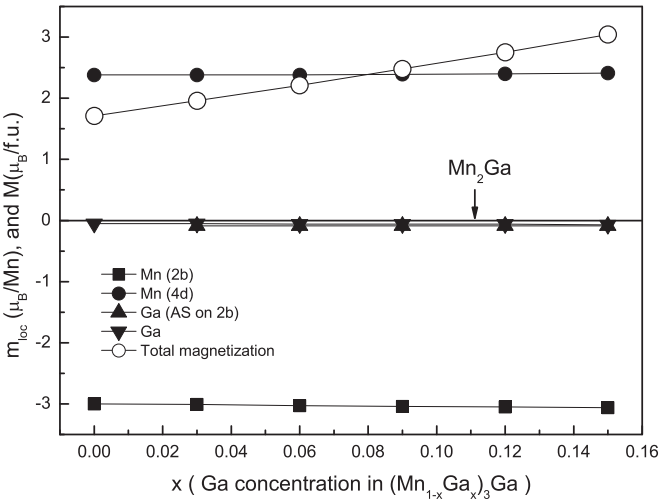

FIG. 4. The local atomic moments and total magnetization of the τ-($Mn_{3-x}Ga_x$) Ga alloy with the Mn-Ga alloy on the 2*b* sites of the DO_{22} structure.

C. Discussion on the possible origin of the magnetic canting

Concerning the possible origin of a small canting of the magnetic moments on the 2*b* sublattice found in the experiment, one can get a good hint from the observation that the midpoint of the nearest-neighbor bond between Mn(2*b*) and Mn(4*d*) has no inversion symmetry. It is obvious since the atoms on different point symmetry positions (also having different magnetic moments) are on the opposite ends of the bond. According to the Moriya criterion [40] this allows for the nonzero relativistic DM interaction between these atomic sites. If the size of the DM interaction exceeds the magnetic anisotropy of either of the nonequivalent Mn sites, this will lead to a canting of the magnetic moment on this site since the DM interaction favors noncollinear configurations of the moments. An analysis of the symmetry suggests that the DM vector of the interaction between first nearest-neighbor (1NN) Mn sites will be directed perpendicular to the face of the unit-cell tetrahedra containing the Mn(2*b*)-Mn(4*d*) bond, which is a mirror symmetry plane. It follows from the Moriya symmetry rule [40] stating that the DM vector has to be perpendicular to the mirror plane containing the bond. It would be interesting to investigate this problem with fully relativistic noncollinear first-principles calculations allowing for the rotation of one sublattice magnetization with respect to the other. Moreover, judging from the calculations, which have been presented in Fig. 18 of Ref. [13], one can see a maximum of the total energy curve with respect to the azimuth angle in between 0° and 180° without specifying the polar angle. This can be a signal of a strong DM interaction. However, if a strong DM interaction is present the total energy will also depend not only on the azimuth, but also on the polar angle, which means that there could be an additional minimum for a canted magnetic configuration.

IV. MAGNETIC ORDERING IN HEXAGONAL ε-Mn_3Ga

The hexagonal crystal structure of Mn_3Ga is shown in Fig. 5(a). The experimental magnetic state of the ε-Mn_3Ga is a triangular structure with a mutual orientation of the neighboring Mn moments of 120° as in the basal magnetic kagome planes as well as between the neighbors on different planes. Indeed such a structure provides a minimum total energy in the fully relativistic calculations by Zhang *et al.* [18] allowing for magnetic noncollinear states. However, the origin of the stabilization of this magnetic structure is still unknown. The main question is whether it is the result of a relativistic MD coupling as was recently suggested [7] or the frustration of the antiferromagnetic exchange interactions on the basal kagome lattices together with antiferromagnetic interplane coupling [18]. In order to investigate this question and to calculate the Néel temperature from first-principles investigations we calculate the interatomic exchange constants for this system.

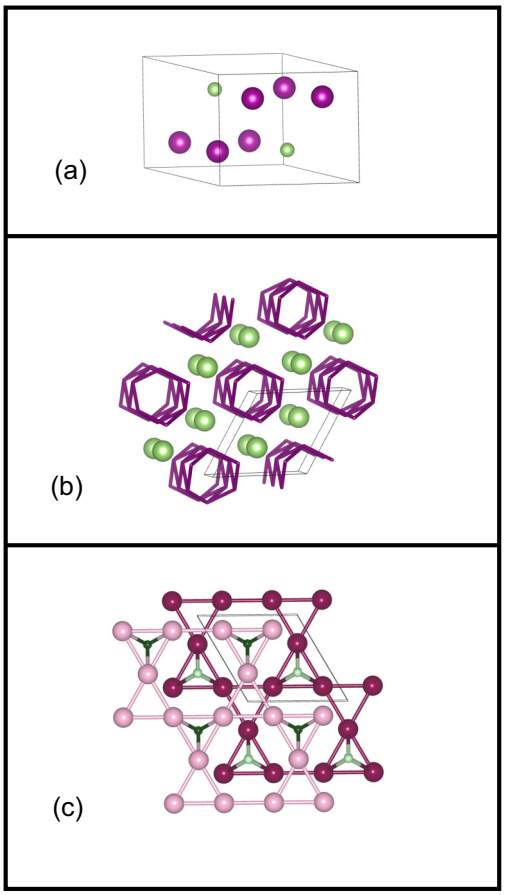

FIG. 5. (a) Hexagonal unit cell of the DO_{19} structure of $MnGa_3$. The large circles are Mn, and the small circles are the Ga atoms, (b) 1NN interplane interactions (bonds) between Mn atoms, and (c) the in-plane nearest-neighbor Mn-Mn bonds and two adjacent basal planes are shown. The connections of Mn to neighboring Ga atoms (small green circles) are also shown, the lighter large circles are Mn on the top kagome plane, and the darker circles are Mn on the bottom kagome plane.

Similar to the tetragonal phase, the ε-Mn_3Ga has well localized magnetic moments in the paramagnetic DLM state of 2.60 μ_B/Mn. In Fig. 5(b), we show the nearest-neighbor interplane bonds between the magnetic Mn atoms in ε-Mn_3Ga. One can see that these bonds form a separated one-dimensional network of connected Mn atoms. These connections are

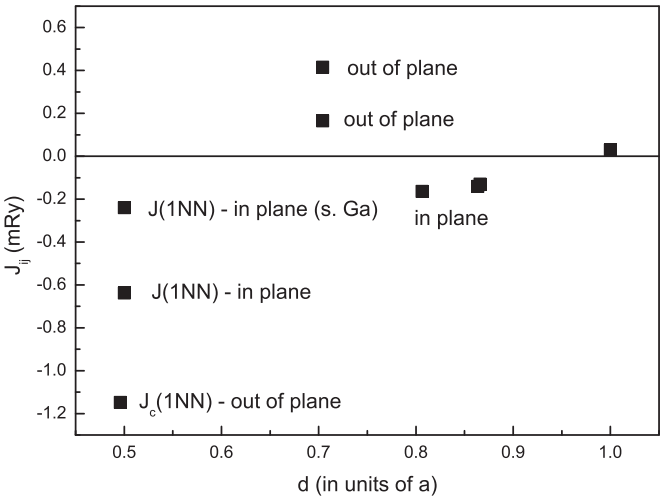

FIG. 6. Calculated magnetic exchange interactions (in mRy) for the ε-Mn_3Ga alloy as a function of interatomic distance (in units of the lattice constant a). (s. Ga) stands for the in-plane interaction between Mn having a shared nearest-neighbor Ga atom.

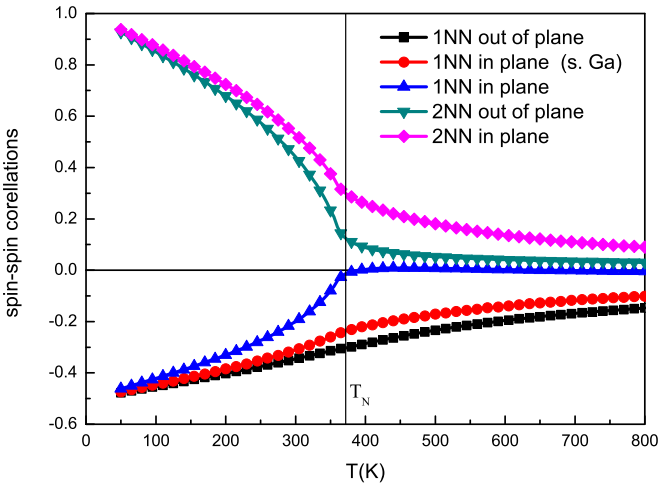

FIG. 7. Calculated spin-spin correlations functions for several Mn coordination shells in ε-Mn_3Ga. The 1NN in-plane (s. Ga) stands for the in-plane shell where Mn has a shared nearest-neighbor Ga atom.

such that each Mn interacts with two Mn atoms on the top kagome plane and with two on the bottom one. Since the corresponding magnetic exchange interaction is the strongest and antiferromagnetic (see Fig. 6), this leads to the frustration effect. This interaction is inducing antiferromagnetic order between the Mn basal planes, however, to be fully energetically satisfied, such a magnetic configuration needs a ferromagnetic arrangement of the Mn atoms in the isolated triangles of the kagome planes since they share the same Mn out-of-plane neighbors. The latter condition is in conflict with in-plane antiferromagnetic interactions between Mn atoms within these triangles. Although they are about four times smaller in magnitude than the strongest ones, nevertheless they are large enough to destroy a noncollinear arrangement in the planes. The in-plane 1NN interactions are different between Mn in the triangles of the kagome planes due to the presence of Ga in the adjacent layers. This is shown in Fig. 5(c) where we show the in-plane NN bonds in two neighboring basal layers. The presence of Ga partitions the kagome planes into triangles with different exchange interactions between sites. The calculated in-plane interaction between Mn with shared Ga neighbors appears to be also antiferromagnetic and larger than between Mn without Ga (-0.23 and -0.64 mRy, respectively). This interaction provides the connection between strongly interacting triangles and ensures the 120° orientation between neighboring Mn moments belonging to different Mn networks as shown in Fig. 5(b). As for the triangles without shared Ga, the triangular structure is a result of the competition between a strong 1NN interplane and a small 1NN kagome-plane interaction as well as a strong (0.41-mRy) ferromagnetic 2NN-inter-plane coupling. Therefore, one can conclude that the triangular structure is the result of both the *geometrical* frustration and the frustration due to competing exchange interactions.

The qualitative consideration given above is fully supported by Monte Carlo simulations with the exchange interactions presented in Fig. 6. We find the magnetic ordering temperature to be about 370 K, which is in good agreement with experiment, 440 K [4]. Similar to the case of the τ phase, there is a 10%–20% underestimation of the Néel temperature, probably due to the same reasons as discussed in the previous section. The system is ordered in a triangular magnetic state in full agreement with experiment. Since the interactions in the system are frustrated we find massive short-range magnetic order effects above the Néel temperature. These effects are presented in Fig. 7 where we plot the calculated spin-spin correlation function for different nearest-neighbor shells defined as

$$c(n) = \frac{1}{N}\sum_i \frac{1}{N_n}\sum_{\vec{R}_n} \langle \vec{e}_{\vec{R}_i}\vec{e}_{\vec{R}_i+\vec{R}_n}\rangle, \qquad (2)$$

where the first sum runs over N translation vectors of the DO_{19} lattice $\vec{R}_i$, the second sum is taken over the N_n translation vectors, $\vec{R}_n$ spans the nth shell connecting Mn, and $\langle\ \rangle$ stands for the statistical average. These functions also determine the average angle between the moments on the respective shells $\langle\varphi_n\rangle = \arccos[c(n)]$, and thus they are good accounts for the short-range order effects. We note that these correlation functions are calculated for each Mn site in the lattice basis. For the present case of ε-Mn_3Ga we find them to be equal for all different sublattices.

At low temperatures, the correlations functions for the 1NN shells have their ground-state values for the triangular structure, which correspond to a mutual angle of 120° [$c(n) = -0.5$]. The 2NN in-plane and interplane planes are connecting the same positions in different unit cells with values of $c(n) = 1.0$ in the ground state. One can also see in Fig. 7 that very strong short-range order effects exist in the temperature range well above Néel for the coordination shells with large exchange interactions (see Fig. 6). The neighboring moments within the triangles of the kagome planes, which have no shared Ga [see Fig. 5(c)] remain almost uncorrelated down to a temperature where long-range magnetic order starts to develop.

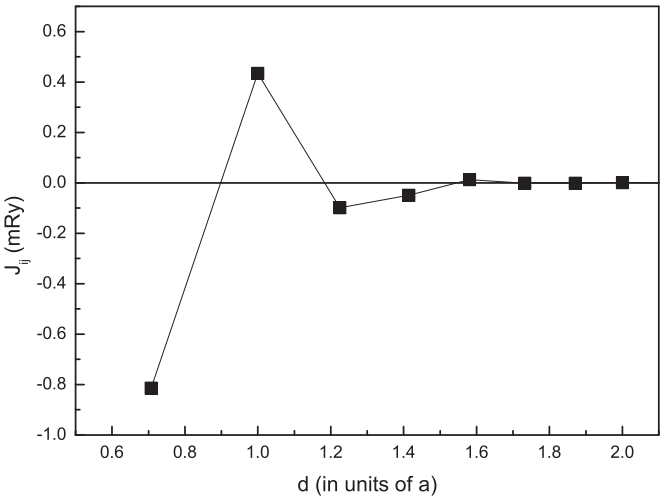

FIG. 8. Calculated magnetic exchange interactions (in mRy) for a fcc random $Mn_{75}Ga_{25}$ alloy as a function of interatomic distance (in units of the lattice constant a).

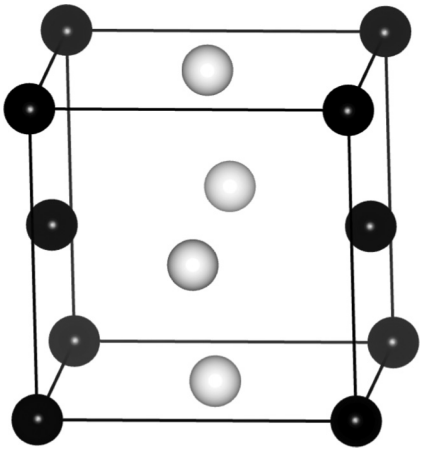

FIG. 9. Derived antiferromagnetic structure of the fcc random $Mn_{75}Ga_{25}$ alloy. The dark circles are spin-up atoms, and the white circles are spin-down atoms. The structure is alternating FM planes along the (100) direction (AFM-1).

V. MAGNETISM OF RANDOM fcc $Mn_{75}Ga_{25}$

The cubic phase of Mn_3Ga was recently produced as a random alloy in the fcc structure [24]. It was found to be magnetically ordered at room temperature with zero total magnetization. Although a clear magnetic phase transition point has not been observed, a large anomaly in the measured magnetization in an applied magnetic field was found around 420 K. Yet, the authors of Ref. [24] have not ruled out the possibility of a random freezing of spins around this temperature (instead of an order-disorder magnetic phase transition) due to the atomically disordered nature of the Mn_3Ga ribbons. The *ab initio* calculations [24], performed for a 32 quasirandom atomic supercell to model substitutional atomic disorder, predict a compensated antiferromagnetic ground state indicating a strong AFM nearest-neighbor coupling.

Here, we perform CPA first-principles calculations of a random $Mn_{75}Ga_{25}$ alloy and find that Mn has a well-defined local moment in the paramagnetic state of 2.44 μ_B, which is similar to those in ordered hexagonal and tetragonal phases. The calculated exchange interactions are shown in Fig. 8. One can see that in addition to the strong 1NN AFM interaction found previously [24], there is a very strong ferromagnetic interaction at the second coordination shell. In general, the fcc lattice is frustrated with respect to the nearest-neighbor AFM interactions, and there exist four possible kinds of collinear AFM structures on a fcc lattice, some of them highly frustrated [25,26]. According to the well-known $(J_{1NN}, J_{2NN}, J_{3NN})$ phase diagram of the magnetic fcc lattice as given by Moran-Lopez *et al.* [26] the calculated exchange interactions (Fig. 8) correspond to a stabilization of the so-called AFM-1 type of magnetic order on the atomically *ordered* fcc lattice (see Fig. 9). Our Monte Carlo simulations are performed on the *disordered* fcc lattice where 25% of the lattice magnetic sites were left empty and are distributed fully randomly and indeed predict a phase transition to the magnetically ordered state of the AFM-1 kind (Fig. 9) at a temperature of 260 K. Again, we underestimate the Néel temperature as compared to the experiment, and we note that this underestimation is slightly larger than in the case of the ordered phases discussed in the previous sections. This shortcoming might be due to some effects of the atomic short-range order in the actual Mn_3Ga ribbons since they are produced by long annealing at the high temperatures.

VI. CONCLUSIONS

The presented study of the finite-temperature magnetic properties of all three stable phases of Mn_3Ga in the same first-principles framework (DLM model, magnetic exchange interactions from the magnetic force theorem calculations, and statistical Monte Carlo simulations) allows us to see similarities and differences between their magnetic properties. In all three phases, Mn has a robust local magnetic moment of 2.4–2.6 μ_B in the high-temperature paramagnetic state. The leading nearest-neighbor interactions also have similar magnitudes ~ -1.2 mRy in the τ and ε phases and ~ -0.8 mRy in the fcc random alloy (see Table I). The further similarity

TABLE I. The Mn magnetic moment in the paramagnetic DLM state, first nearest-neighbor exchange interaction, calculated, and experimental ordering temperatures. Moments for the hexagonal phase are given for 2a and 4d sites.

Mn_3Ga structure	Moment Mn, μ_B in the PM state	J (1NN) mRy	Tc (K) calculated	Tc (K) experimental
Hexagonal	2.6	1.17	370	440
Tetragonal	2.43/2.53	1.21	685	~770
Disordered fcc	2.44	0.8	260	420

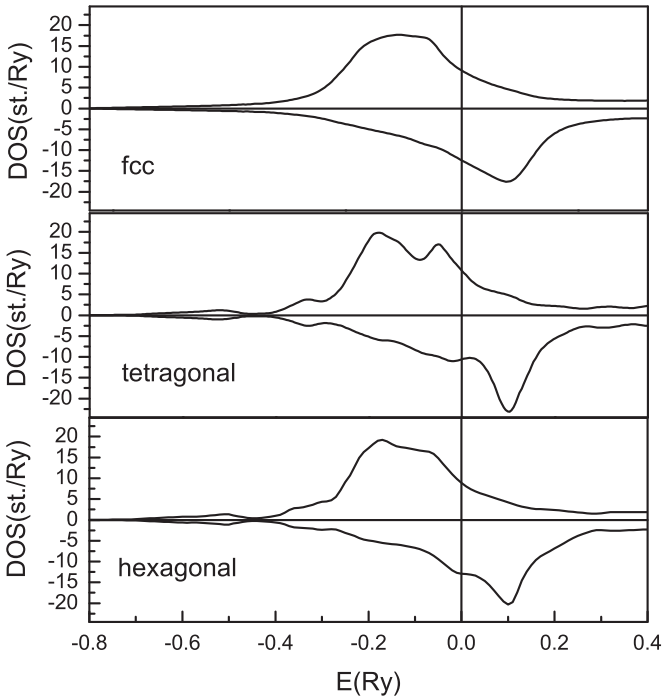

FIG. 10. Calculated atom projected Mn density of states of Mn_3Ga alloys for three modifications: disordered fcc (upper panel), tetragonal (middle panel), and hexagonal (lower panel). The DOS is given in states/Ry per spin per Mn atom for majority and minority spin channels in the disordered local moment state.

can be seen from the Mn density of states (DOS) calculated in the paramagnetic regime, which is shown in Fig. 10. One can see the similar size of the exchange splitting of the majority and minority spin channels. The only essential difference is a smearing out of the DOS for the fcc alloy induced by the chemical disorder effects. The essential differences in the ordering temperatures among tetragonal and two other phases are partially due to the geometrical magnetic frustration of the hexagonal and fcc lattices. The frustration effects lead not to the noncollinear order in the hexagonal phase but to a collinear order in the disordered fcc phase. The origin of the triangular order in the hexagonal phase of Mn_3Ga with DO_{19} symmetry may be understood and derived from the nonrelativistic isotropic exchange interactions, but, as we have argued, the understanding of the canted noncollinear structure in the tetragonal alloy may require the relativistic DM interaction. Although off-stoichiometry (Mn deficiency) leads to pronounced changes in the total magnetization of the tetragonal phase, we find, similar to the situation in other related materials [41,42] that a moderate off-stoichiometry and associated partial atomic disorder has little effect on the Mn local atomic moments and interatomic exchange interactions in both the tetragonal and the hexagonal phases.

ACKNOWLEDGMENT

This work has been supported by the Austrian Science Fund (FWF) within the ViCoM Project No. F4109-N28.

[1] *Handbook of Spin Transport and Magnetism*, edited by E. Y. Tsymbal and I. Zutic (CRC, London/New York, 2012).
[2] H. Kurt and J. M. D. Coey, in *Heusler Alloys: Properties, Growth, Applications,* edited by C. Felser and A. Hirohata (Springer, Heidelberg/London/New York, 2016), pp. 157–192.
[3] J. M. D. Coey, J. Phys.: Condens. Matter **26**, 064211 (2014).
[4] E. Kren and G. Kadar, Solid State Commun. **8**, 1653 (1970).
[5] H. Niida, T. Hori, Y. Yamaguchi, and Y. Nikagawa, J. Appl. Phys. **73**, 5692 (1993).
[6] H. Kurt, K. Rode, M. Venkatesan, P. Stamenov, and J. M. D. Coey, Phys. Status Solidi B **248**, 2338 (2011).
[7] H. Kurt, K. Rode, H. Tokuc, P. Stamenov, M. Venkatesan, and J. M. D. Coey, Appl. Phys. Lett. **101**, 232402 (2012).
[8] L. Szunyogh, B. Lazarovits, L. Udvardi, J. Jackson, and U. Nowak, Phys. Rev. B **79**, 020403 (2009).
[9] J. Winterlik, B. Balke, G. H. Fecher, C. Felser, M. C. M. Alves, F. Bernardi, and J. Morais, Phys. Rev. B **77**, 054406 (2008).
[10] S. Mizukami, F. Wu, A. Sakuma, J. Walowski, D. Watanabe, T. Kubota, X. Zhang, H. Naganuma, M. Oogane, Y. Ando, and T. Miyazaki, Phys. Rev. Lett. **106**, 117201 (2011).
[11] L. Zhu and J. Zhao, Appl. Phys. A **111**, 379 (2013).
[12] S. Mizukami, T. Kubota, F. Wu, X. Zhang, T. Miyazaki, H. Naganuma, M. Oogane, A. Sakuma, and Y. Ando, Phys. Rev. B **85**, 014416 (2012).
[13] K. Rode, N. Baadji, D. Betto, Y.-C. Lau, H. Kurt, M. Venkatesan, P. Stamenov, S. Sanvito, J. M. D. Coey, E. Fonda, E. Otero, F. Choueikani, P. Ohresser, F. Porcher, and G. André, Phys. Rev. B **87**, 184429 (2013).
[14] D. Kim, J. Hong, and L. Vitos, Phys. Rev. B **90**, 144413 (2014).
[15] J. Kübler, J. Phys.: Condens. Matter **18**, 9795 (2006).
[16] B. Balke, G. H. Fecher, J. Winterlink, and C. Felser, Appl. Phys. Lett. **90**, 152504 (2007).
[17] S. Chadov, S. W. D'Souza, L. Wollmann, J. Kiss, G. H. Fecher, and C. Felser, Phys. Rev. B **91**, 094203 (2015).
[18] D. Zhang, B. Yan, S.-C. Wu, J. Kübler, G. Kreiner, S. S. P. Parkin, and C. Felser, J. Phys.: Condens. Matter **25**, 206006 (2013).
[19] S. Tomiyoshi, Y. Yamaguchi, and T. Nagamiya, J. Magn. Magn. Mater. **31–34**, 629 (1983).
[20] T. Nagamiya, S. Tomiyoshi, and Y. Yamaguchi, Solid State Commun. **42**, 385 (1982).
[21] S. Wurmehl, H. C. Kandpal, G. H. Fecher, and C. Felser, J. Phys.: Condens. Matter **18**, 6171 (2006).
[22] L. Wollmann, S. Chadov, J. Kübler, and C. Felser, Phys. Rev. B **92**, 064417 (2015).
[23] H. Kurt, K. Rode, P. Stamenov, M. Venkatesan, Y.-C. Lau, E. Fonda, and J. M. D. Coey, Phys. Rev. Lett. **112**, 027201 (2014).
[24] P. Kharel, Y. Huh, N. Al-Aqtash, V. R. Shah, R. F. Sabirianov, R. Skomski, and D. J. Sellmyer, J. Phys.: Condens. Matter **26**, 126001 (2014).
[25] T. Yildirim, A. B. Harris, and E. F. Shender, Phys. Rev. B **58**, 3144 (1998).

[26] J. L. Moran-Lopez, R. Rodriiguez-Alba, and F. Aguilera-Granja, J. Magn. Magn. Mater. **131**, 417 (1994).
[27] J. P. Perdew and Y. Wang, Phys. Rev. B **45**, 13244 (1992).
[28] I. A. Abrikosov and H. L. Skriver, Phys. Rev. B **47**, 16532 (1993).
[29] A. V. Ruban and H. L. Skriver, Comput. Mater. Sci. **15**, 119 (1999).
[30] A. I. Lichtenstein, M. I. Katsnelson, V. P. Antropov, and V. A. Gubanov, J. Magn. Magn. Mater. **67**, 65 (1987).
[31] A. V. Ruban, S. I. Simak, S. Shallcross, and H. L. Skriver, Phys. Rev. B **67**, 214302 (2003).
[32] B. L. Gyorffy, A. J. Pindor, J. Staunton, G. M. Stocks, and H. Winter, J. Phys. F: Met. Phys. **15**, 1337 (1985).
[33] S. Khmelevskyi and P. Mohn, Appl. Phys. Lett. **93**, 162503 (2008).
[34] V. M. T. S. Barthem, C. V. Colin, H. Mayaffre. M.-H. Julien, and D. Givord, Nat. Commun. **4**, 2892 (2013).
[35] S. Khmelevskyi, E. Simon, and L. Szunyogh, Phys. Rev. B **91**, 094432 (2015).
[36] B. Alling, A. V. Ruban, and I. A. Abrikosov, Phys. Rev. B **79**, 134417 (2009).
[37] A. V. Ruban, S. Khmelevskyi, P. Mohn, and B. Johansson, Phys. Rev. B **75**, 054402 (2007).
[38] Y. O. Kvashnin, O. Grånäs, I. Di Marco, M. I. Katsnelson, A. I. Lichtenstein, and O. Eriksson, Phys. Rev. B **91**, 125133 (2015).
[39] S. Khmelevskyi, T. Khmelevska, A. V. Ruban, and P. Mohn, J. Phys.: Condens. Matter **19**, 326218 (2007).
[40] T. Moriya, Phys. Rev. **120**, 91 (1960).
[41] I. Galanakis, K. Özdogan, and E. Sasioglu, Phys. Rev. B **86**, 134427, (2012).
[42] K. Özdogan, E. Sasioglu, and I. Galanakis, J. Appl. Phys. **103**, 023503 (2008).